Ratios of greenhouse gas emissions observed over the Yellow Sea and the East China Sea

Yunsong Liu[a], Lingxi Zhou[a,*], Pieter P. Tans[b], Kunpeng Zang[a,c], Siyang Cheng[a,*]

[a] *State Key Laboratory of Severe Weather, Chinese Academy of Meteorological Sciences (CAMS), Beijing 100081, China*

[b] *Earth System Research Laboratory, National Oceanic and Atmospheric Administration, Boulder, Colorado 80305, USA*

[c] *National Marine Environmental Monitoring Center, Dalian, China*

Abstract

During a cruise of the survey vessel Dongfanghong II on the Yellow Sea and the East China Sea in the spring of 2017 we performed accurate measurements of the mole fractions of carbon dioxide (CO_2), methane (CH_4), carbon monoxide (CO) and nitrous oxide (N_2O) using two types of Cavity Ring-Down Spectrometers (CRDS). The spatial variations of the mole fraction of the four trace gases were very similar. The emission sources of these gases were divided into several regions by using the NOAA HYSPLIT model. Then we analyzed the variations of the ratios of the mole fraction enhancements between every pair of trace gases downwind of these source areas. The ratios showed that the distributions of these trace gases over the Yellow Sea and the East China Sea in the spring were mainly caused by the emissions from Eastern China. The much

* Corresponding authors.
Email addresses: chinalingxi_zhou@163.com (L. Zhou), chinachengsiyang@163.com (S. Cheng).

higher enhancement ratio of $\Delta CO/\Delta CO_2$ and the lower ratio of $\Delta CH_4/\Delta CO$ observed in the air parcels from big cities like Beijing and Shanghai indicated high CO emission from the cities during our time of observation. Compared with the values of NOAA's Marine Boundary Layer (MBL), the ratios of the averages in the air coming from the Northern sector (Russia) were on average closer to the MBL, and the air that stayed over the Yellow Sea and the East China Sea was a mixture of emissions from wide regional areas. The highly variable N_2O data of the air from Qingdao and Shanghai showed much more fluctuation.

Keywords: mole fraction, calibration, source regions, enhancement ratios, shipboard air measurements, major greenhouse gases

1. Introduction

The problems of global warming and climate change are mainly caused by the greenhouse gas increases, and have become one of the most important challenges of the 21st century (Liu et al., 2009). Greenhouse gases are pervasively produced by human activities, such as coal combustion, vehicle traffic, heating/cooling and industrial processes. The Asian continent has become the largest source of anthropogenic pollutants. Emissions to the atmosphere have rapidly increased recently as a result of the economic growth in Asian countries, especially China (Sakata et al., 2013; Zhang et al., 2017). The industrialization and energy consumption in China are increasing rapidly, and the total CO_2 emissions from fossil-fuels and cement production increased from 1.4 billion (10^9) metric ton carbon (GtC) in 2004 to 2.8 GtC in 2014 according to the data of Carbon Dioxide Information Analysis Center (Boden and

Andres, 2017). This is regarded as the main reason for a sharp increase in continental Asian air pollution (Junker et al., 2009).

The platforms for observations of the greenhouse gases and their temporal and spatial variations around the world are ground-based stations (Cheng et al., 2017; Gomez-Pelaez et al., 2013; Zellweger et al., 2016), aircraft (Chen et al., 2010; Daube et al., 2002; Machida et al., 2008), satellites (Butz et al., 2011; Guo et al., 2017; Wunch et al., 2017), and ships (Feely et al., 2006; Schuster et al., 2009). Observation data are essential for atmospheric inversion methods to estimate regional sources and sinks, regional fluxes and the transport of the greenhouse gases (Deng et al., 2014; Peylin et al., 2013; Sawa et al., 2012).

Akira Wada et al. (2007; 2011) analyzed seasonal and geographical variations of the enhancement ratios of trace gases and found that the Asian continental pollution was influenced by the seasonal variations of the emission ratios in the source regions, with increased fluxes of methane (CH_4) in summer and carbon monoxide (CO) in winter. The Asian influence on CO in the North Pacific troposphere is at a maximum during spring and at a minimum during summer (Liang et al., 2004), and observed and simulated concentrations of CO_2 in the Asian outflow would imply increases in Chinese anthropogenic CO_2 emissions (Suntharalingam et al., 2004).

In this paper, we study the data of carbon dioxide (CO_2), methane (CH_4), carbon monoxide (CO), and nitrous oxide (N_2O) obtained on the ship over the Yellow Sea lying between northeastern China and the Korean Peninsula (Li et al., 2016) and the East China Sea (32.07° N, 125.10° E) in the spring (Han et al., 2015). We designed and built a ship-based continuous observation system for the main atmospheric greenhouse gases and CO in order to explore the

factors that affected the distribution of the gases. Firstly we defined the stability of the two analyzers during the cruise and then we analyzed the mole fraction distribution of the four gas species over the Yellow Sea and the East China Sea during the cruise. We used two methods to calculate the enhancement ratios for every pair of gases, and analyzed the results for understanding emission characteristics of the source regions.

2. Observation

2.1. Observation area

We performed accurate measurements of CO_2, CH_4, CO, and N_2O in air during an oceanographic cruise on board the survey vessel Dongfanghong II, organized by the Ocean University of China from 27 March 2017 to 15 April 2017. The ship track is shown in Figure 1.

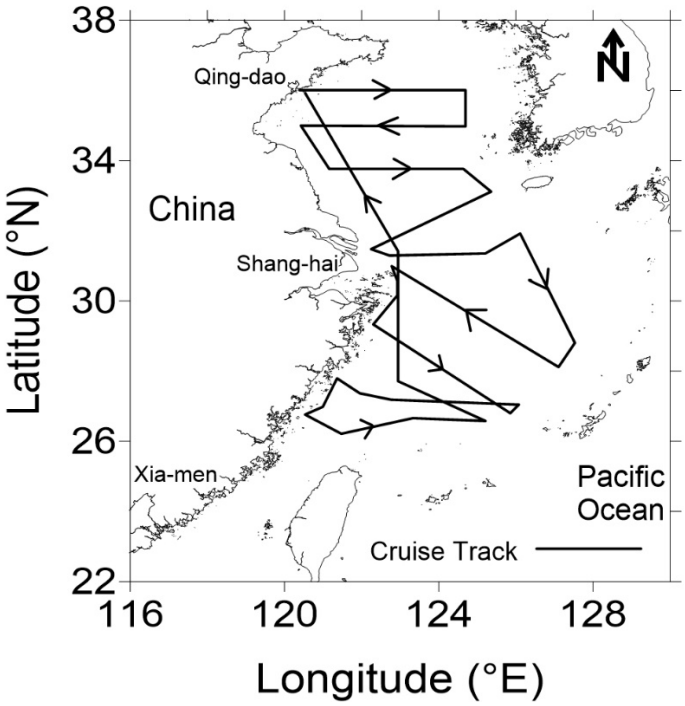

Fig. 1. Cruise track between the Pacific Ocean and the Asian continent. The survey vessel sailed from Qingdao and finally returned to Qingdao.

2.2. Observation methods

We took a Picarro G5101i analyzer for N_2O, and a Picarro G2401 analyzer for CO_2, CH_4, and CO, as well as four high pressure calibration standard gas cylinders, each containing very accurately known amounts of the four gases in air, from 394.24 to 434.12 micromol/mol (ppm) for CO_2, from 1935.00 to 2288.89 nanomol/mol (ppb) for CH_4, from 317.20 to 878.51 ppb for CO, and from 309.75 to 609.24 ppb for N_2O. The calibration of these standard gases was propagated by the Chinese Academy of Meteorological Sciences, China Meteorological Administration (CAMS-CMA). The CAMS standard gases were in turn calibrated using the primary standards of the World Meteorological Organization Global Atmospheric Watch (WMO-GAW), maintained by NOAA/ESRL (www.esrl.noaa.gov/gmd/ccl/; Fang et al., 2014;

Tans and Zellweger, 2014). Sample air was provided by using a sample inlet installed above the top deck, about 10 m in front of the ship's engine exhaust stack. The schematic diagram of the measurement set up was as follows. The 1.0 μm membrane filter between the air inlet and the pump was used to remove particles. One of the air inlets was used as a backup to avoid special situations during the voyage. The sample or standard gas flowed through the eight port multi-position valves into a mass flowmeter which controlled the flow rate at 350 $mL \cdot min^{-1}$, then flowed into a dryer to remove water vapor, a tube filled with magnesium perchlorate ($Mg(ClO_4)_2$). Glass cotton on both sides of the dryer was used to avoid pumping the magnesium perchlorate particles into the analyzers. The cavity pressure of G2401 was maintained at a stable value of 140 torr by the vacuum pump, while the cavity operating pressure of G5101i was at 100 torr (Crosson, 2008; Erler et al., 2015)

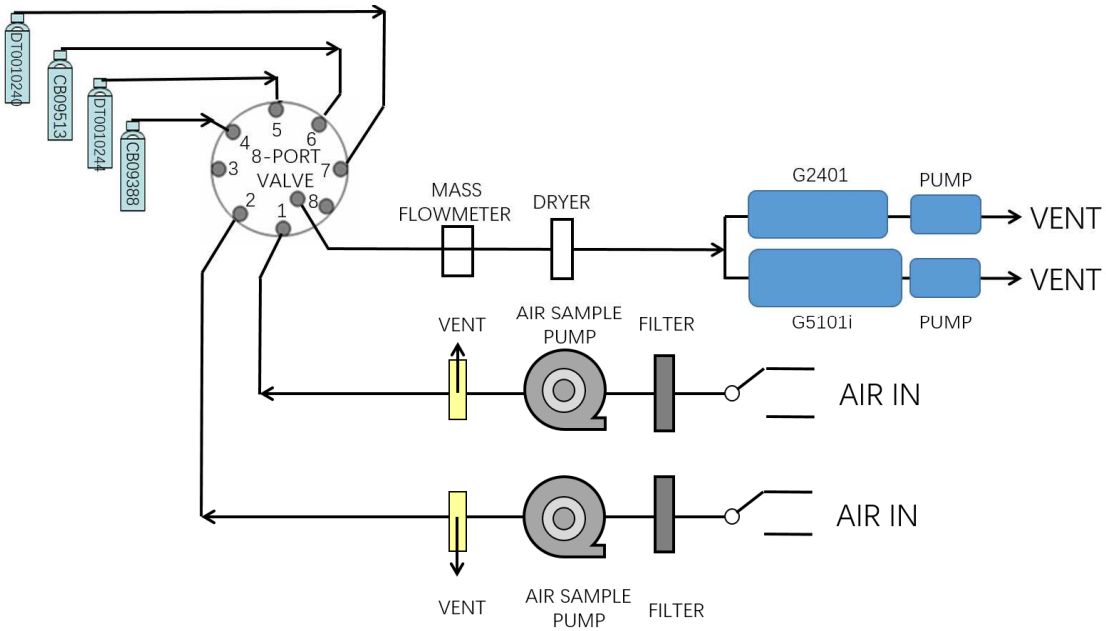

Fig. 2. Schematic diagram (not to scale) of the ship-based atmospheric CO_2, CO, CH_4, and N_2O observation system. The flow rate was controlled at 350 $mL \cdot min^{-1}$ by the mass flowmeter.

2.3. Calibrations

Using the calibration gases, the response functions of the analyzers were calculated 35 times during the whole voyage. The Picarros recorded measurement values approximately every 5 seconds. Every standard gas ran for ten minutes each time, and to ensure complete flushing of the measurement cell only the last 5 minutes of data were used. Then the averages of the stable five minutes of calibration data was calculated for each standard gas. All four standards were used during each calibration to generate a response curve for each instrument over the ranges mentioned above. During sample air measurements, in between the calibrations, the averages of the bracketing calibrated response curves were used to correct the observation data.

Figures 3-6 showed the average difference and standard deviation during the 5 min. averaging periods between the value indicated by the instrument and the known value of the standard gas for all 35 calibrations, for example cylinder number CB09388. The other three standard gases behaved similarly to CB09388, with dips in a few cases at the same times. The uncertainty of the air measurements was larger between times in which successive calibration curves showed a larger change. Compared to the other three gases, CO_2 showed relatively larger changes.

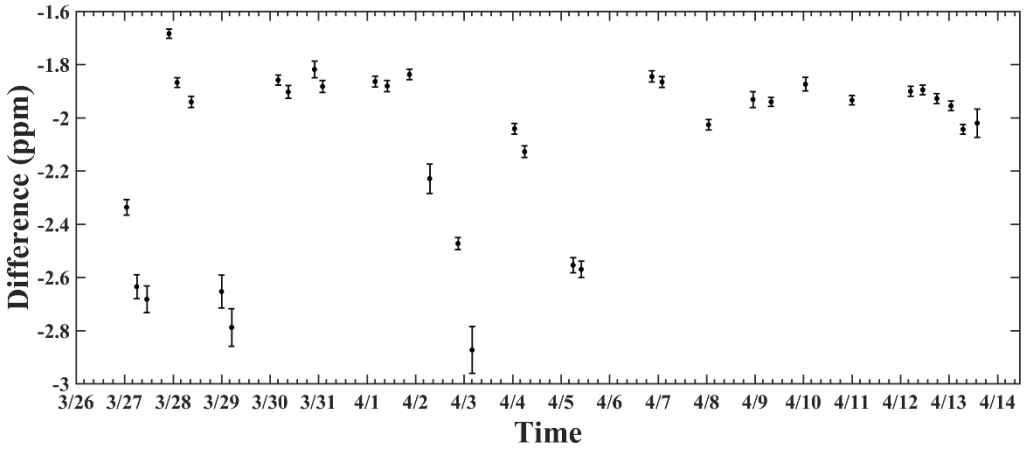

Fig. 3. Stability of successive CO_2 calibrations, the error bars represent the standard deviation of 5-second averages, 35 in total.

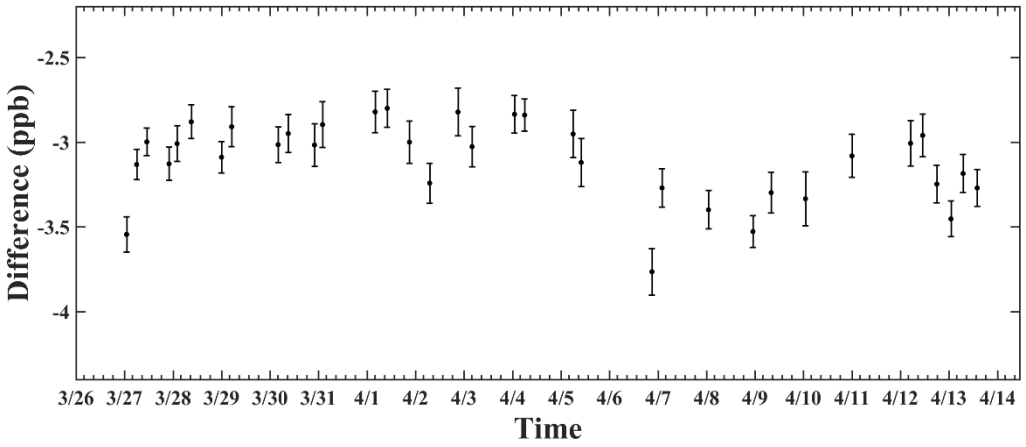

Fig. 4. Stability of successive CH_4 calibrations, the error bars represent the standard deviation of 5-second averages, 35 in total.

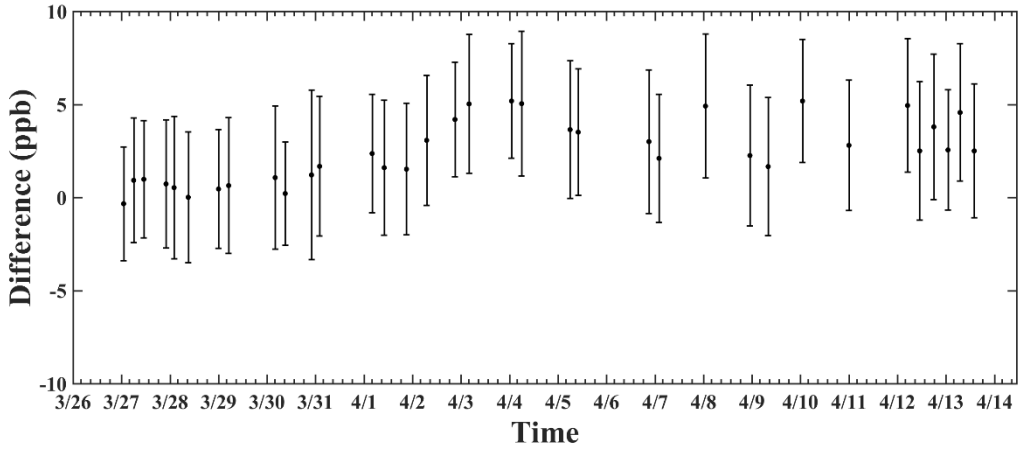

Fig. 5. Stability of successive CO calibrations, the error bars represent the standard deviation of 5-second averages, 35 in total.

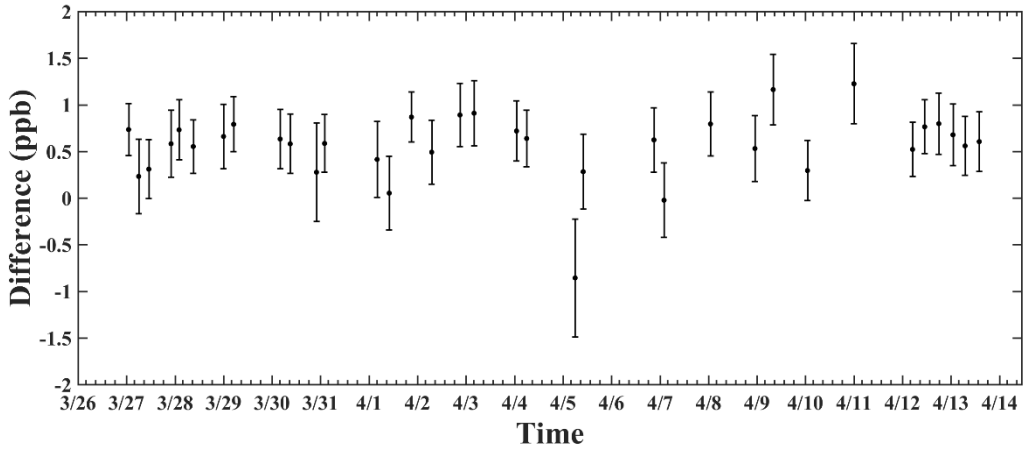

Fig. 6. Stability of successive N_2O calibrations, the error bars represent the standard deviation of 5-second averages, 35 in total.

3. Results

3.1. Observed mole fraction distribution

To avoid interference from the ship's engine exhaust, the data when the ship's speed was less than 3 knots was not used. Occasional contamination from the stack was characterized by very high frequency variability, and we did not use that data either. Fig.7 shows the mole fraction distribution of CO_2 during the voyage. The distributions of the other three gases had similar trends. The data were averaged over each minute and linked to the latitude and longitude. In order to smooth the mole fraction distributions, we calculated hourly average data. Then we used the NOAA HYSPLIT model to generate 72-hour backward air trajectories for each hour with its average longitude and latitude, with the starting point at 300 m altitude. Also, the CO_2, CO, CH_4, and N_2O data were divided into two parts according to the hourly standard deviation, with the dividing lines respectively at 0.88 ppm, 6.35 ppb, 1.15 ppb and 1.48 ppb. Above these values, the data were not very stable so we called them higher variability data while below those values we called them lower variability data. According to the calculated air trajectories, all the data was divided into ten distinct source regions that influenced the data at different times during the cruise. The locations of source regions and regional stations are showed in the Fig. 9. Fig. 8a is an example showing Beijing/Jinan and 8b showing Yellow Sea. The data of the Philippine Sea, at the eastern end of the cruise, were used as the base line for comparing all other data.

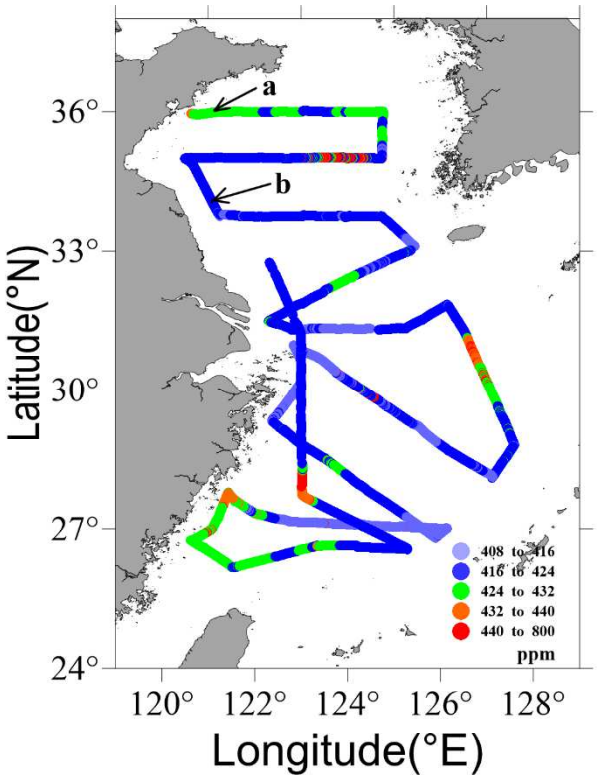

166

167 **Fig. 7.** CO_2 mole fraction distribution as a function of degrees north latitude and east

168 longitude. The point labeled "a" refers to Fig. 8a, and "b" to Fig. 8b, below.

169

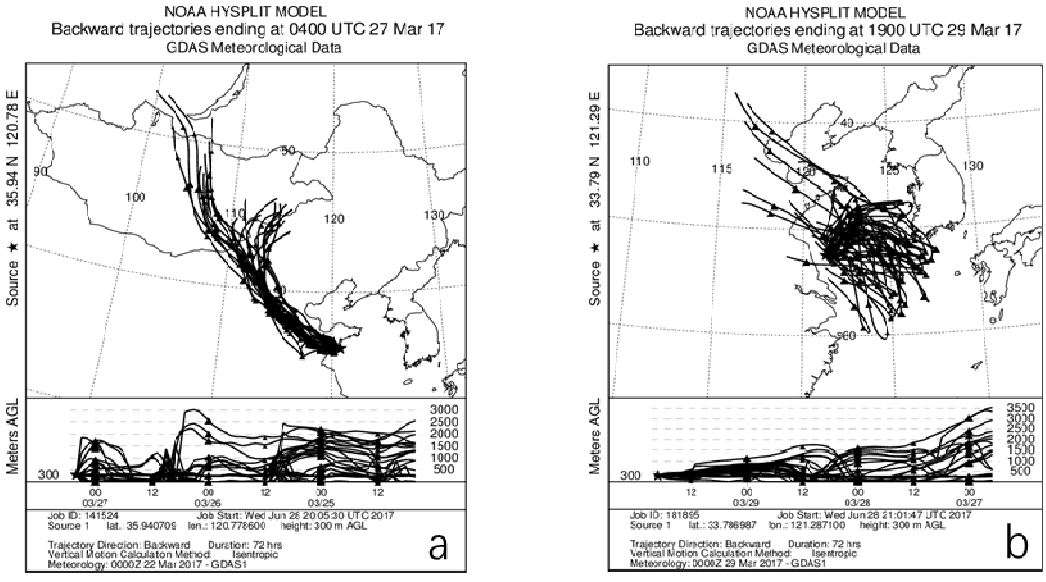

170

171 **Fig. 8.** Three-day air back-trajectories of two locations, a (35.94° N, 120.78° E) and b

172 (33.77° N, 121.29° E).

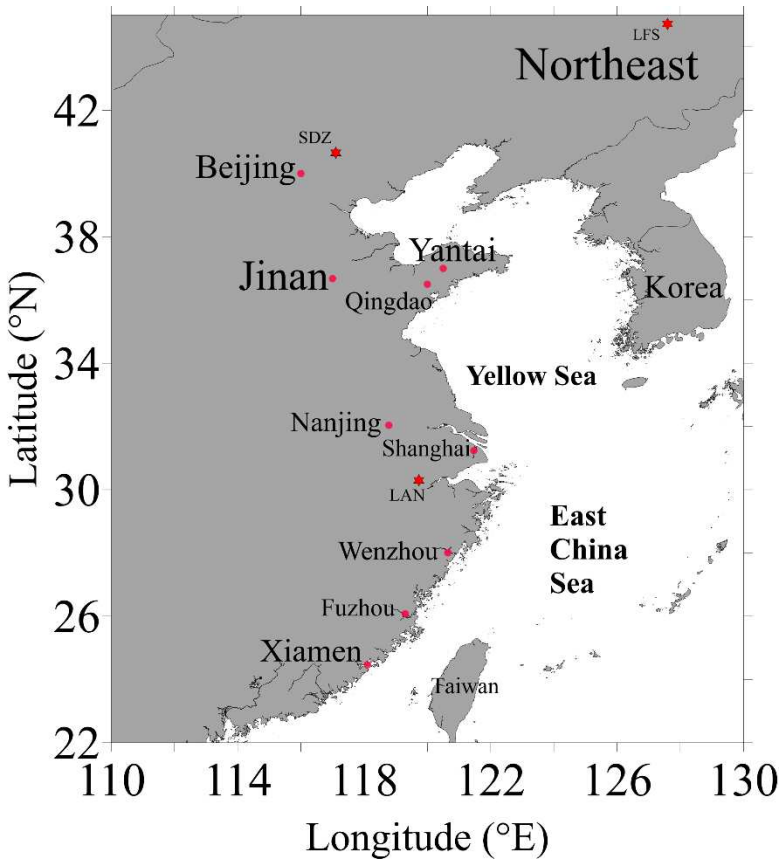

Fig. 9. The locations of the source reigns and regional stations.

3.2. Ratios of mole fraction enhancements

Figures 10 to 15 show the ratios of the observed mole fraction enhancements relative to the Philippine Sea, pairwise for ΔCO_2, ΔCO, ΔCH_4, and ΔN_2O. The average values for the Philippine Sea observed during the cruise are 410.7 ppm, 113 ppb, 1896 ppb, and 332.5 ppb, respectively. NOAA's Marine Boundary Layer (MBL) values (Masarie, 1995), representative of large ocean areas, at the same latitude zone and during the cruise, were 410.7 ppm, 128 ppb, 1911 ppb, and 330.2 ppb respectively. This indicates that our Philippine Sea data is a good reference for this study. We used two different methods. In the first we plotted enhancements for individual hourly averages of a pair of species directly against each other for each source

region, and we determined the slope, without paying attention to the average offsets (blue bars), with the aim to emphasize more recent emissions that had undergone less mixing and may have had larger hour-to-hour variations. For the purpose of calculating uncertainties from the statistics, the hourly averages have the advantage that successive hours are independent of each other whereas successive one minute averages are often very close together, and can not be considered to be independent measurements. The blue and orange columns show lower variability data and higher variability data respectively, again to try to separate emissions that were perhaps closer to the measurement point from those further away. The heights of the bars are the slopes of the relations between every two gas species. The slope is obtained by first fitting $\Delta Y = a\Delta X + b$ assuming errors only on the y-axis, and by then fitting $\Delta X = \frac{\Delta Y}{a'} - \frac{b'}{a'}$ assuming errors only on the x-axis. This gives different values for the slopes a and a'. We take the geometric mean of a and a', keeping track of whether the slope is positive or negative, as below.

$$c = sign(a) * \sqrt{aa'} \quad (1)$$

The difference between the two slopes a and a' provides a measure of the uncertainty of c (denoted as "u(c)"), namely ± (a-a')/2, which is plotted on each bar in Figs 10-15.

The gray and yellow column values show the ratios (Y) of the averages (denoted by the overbar ¯) of the separate enhancements of two species X_1 and X_2, namely $Y = \frac{\overline{\Delta X_1}}{\overline{\Delta X_2}}$, for the lower variability data (gray) and the higher variability data (yellow), respectively. The uncertainty is estimated as the relative uncertainty of a product or quotient, as in the GUM 1995, as follows:

$$\frac{u(Y)}{Y} = \sqrt{\left[\frac{u(\overline{\Delta X_1})}{(\overline{\Delta X_1})}\right]^2 + \left[\frac{u(\overline{\Delta X_2})}{(\overline{\Delta X_2})}\right]^2} \quad (2)$$

in which the standard error of the mean for both species is

$$[u(\overline{\Delta X_1})]^2 = \frac{\sum_{i=1}^{n}(\Delta x_{1i} - \overline{\Delta x_1})^2}{n(n-1)} \quad and \quad [u(\overline{\Delta X_2})]^2 = \frac{\sum_{i=1}^{n}(\Delta x_{2i} - \overline{\Delta x_2})^2}{n(n-1)} \qquad (3)$$

and where ΔX_1, ΔX_2 can be one of ΔCO_2, ΔCO, ΔCH_4, ΔN_2O.

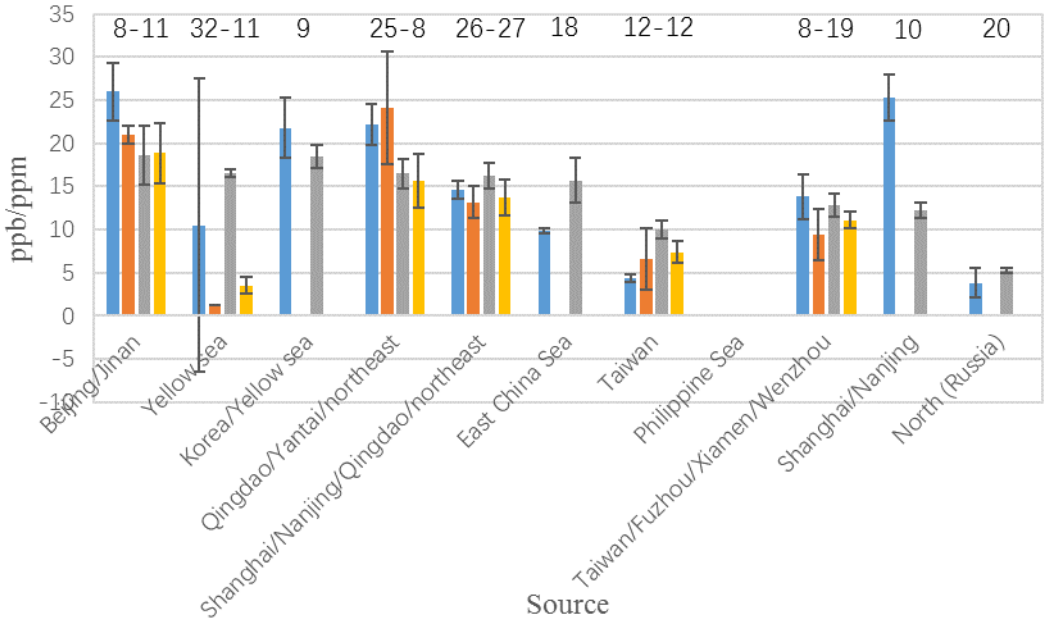

Fig. 10. The enhancement ratios of $\Delta CO/\Delta CO_2$. For all plots 10-15, the numbers n1-n2 above the bars give the number of hourly averages used for each region, n1 for lower variability data (blue and gray bars), n2 for higher variability data (orange and yellow bars). We do not plot bars when they are based on 5 or fewer hourly averages.

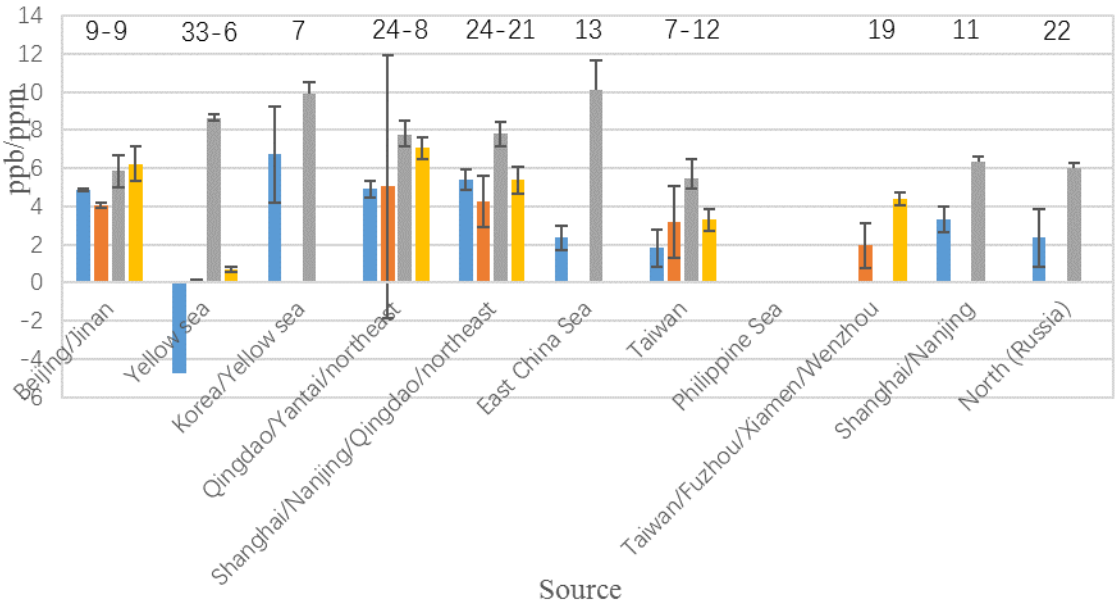

216

217 **Fig. 11.** The enhancement ratios of $\Delta CH_4/\Delta CO_2$.

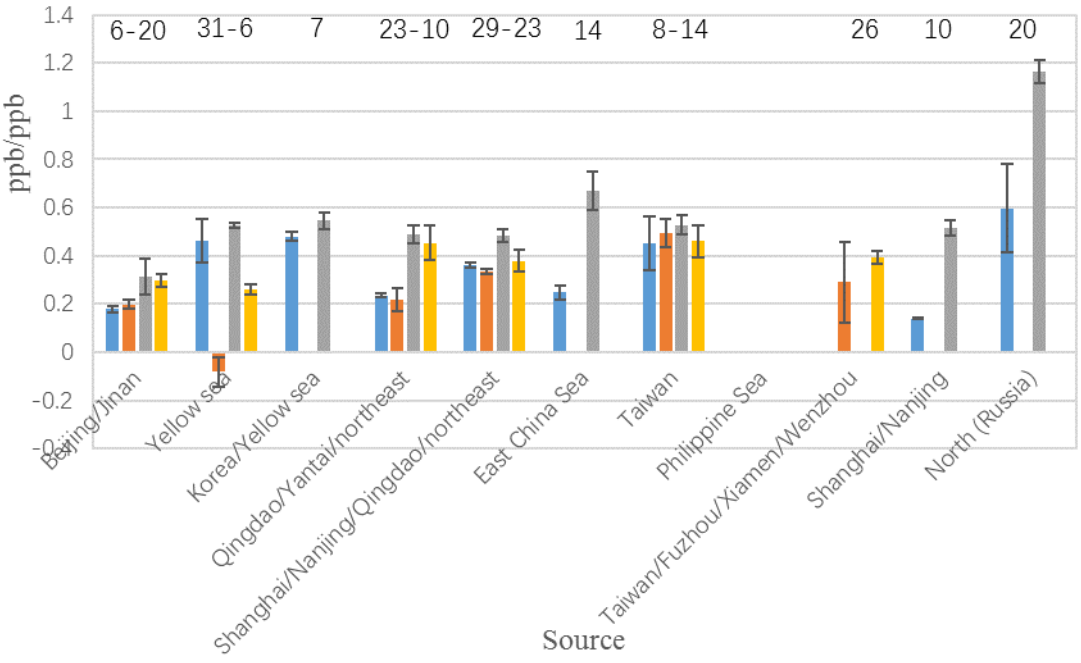

218

219 **Fig. 12.** The enhancement ratios of $\Delta CH_4/\Delta CO$.

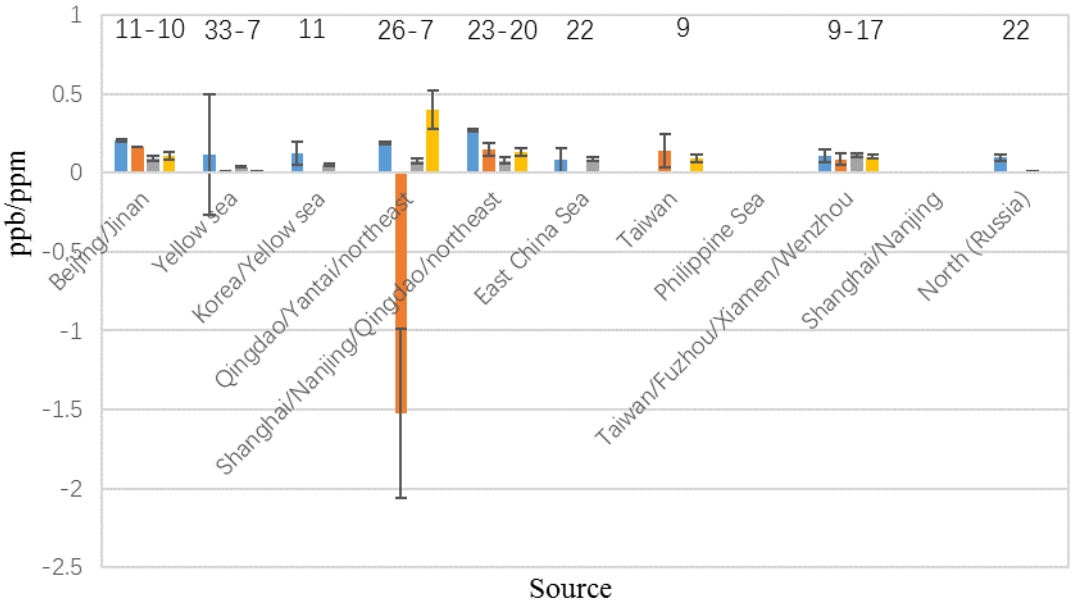

220

221 **Fig. 13.** The enhancement ratios of $\Delta N_2O/\Delta CO_2$.

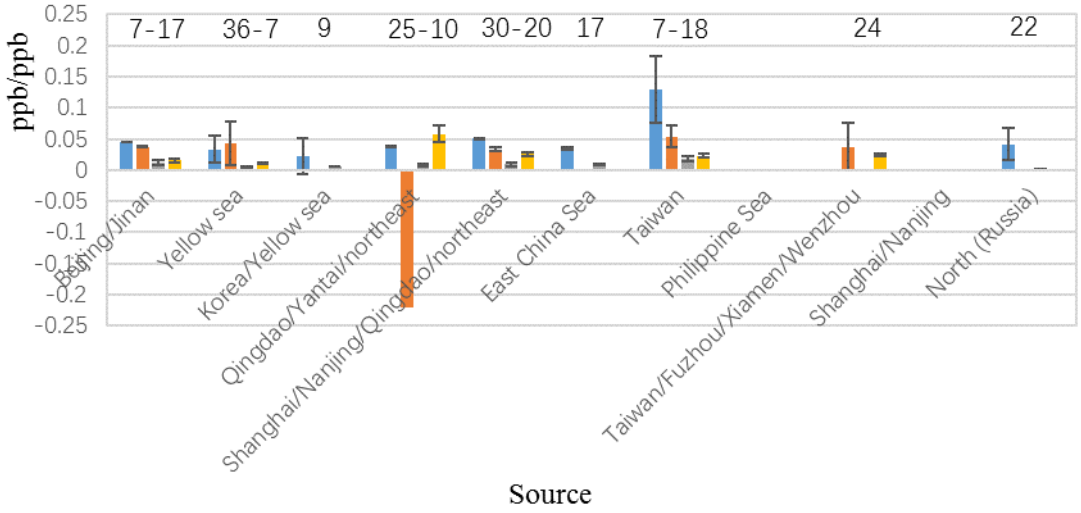

222

223 **Fig. 14.** The enhancement ratios of $\Delta N_2O/\Delta CH_4$.

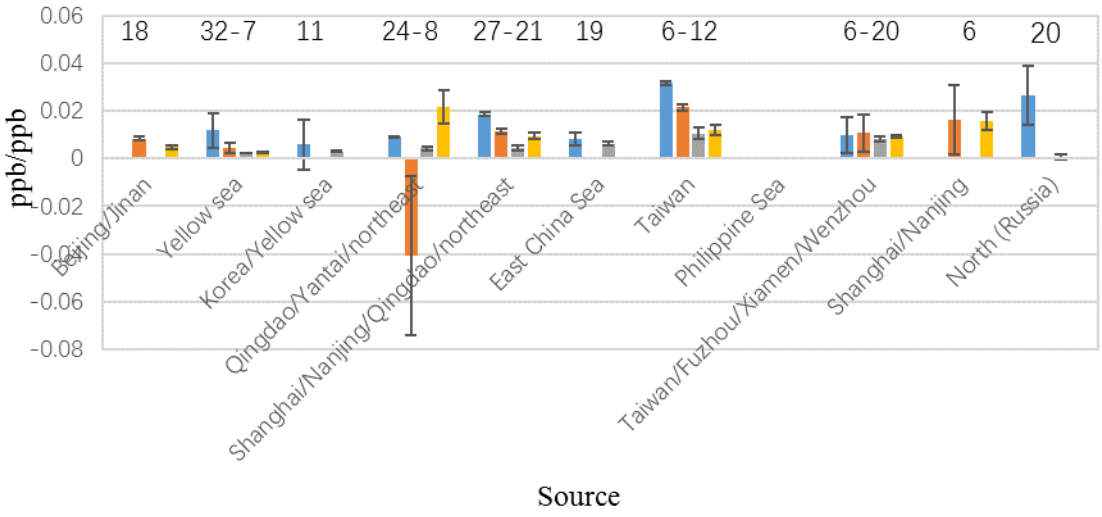

Fig. 15. The enhancement ratios of $\Delta N_2O/\Delta CO$.

3.3. Discussions

We will briefly discuss some characteristics of the ratios of mole fraction enhancements as shown in Figs. 10-15 for individual source regions because they are a measure of their relative emissions during the time period of the cruise.

3.3.1. Beijing Jinan

In both lower and higher variability data the correlation between every pair of gases is strong. The average mole fraction enhancements of the four gases CO_2, CO, CH_4, N_2O in the low-noise case were respectively 13.6 ppm, 244.7 ppb, 81.9 ppb, 1.1 ppb higher than the base values and higher than for other source regions except for N_2O and CH_4. CO emissions are very high, and likely caused by traffic. They were 3-4 times higher than CH_4 emissions. The

239 bars show ratios of emissions, so that if we have a trustworthy estimate for one of them, for
240 example CO_2, then we have estimates for the other gases. The higher variability data was
241 similar to the lower variability data. CO_2 emissions from burning fossil fuels and factories, as
242 well as CH_4 emissions from landfills, made up 97% GHGs of Beijing in 2014 (Li et al., 2017).
243 Li et al. gathered and calculated the results of the inventory of Beijing GHG emissions
244 including CO_2, CH_4 and N_2O for 2014. We use the Li et al.'s estimate of CO_2 emission from
245 fossil fuels and the ratios to give us an estimate for CH_4 and N_2O, about 355 kt/yr
246 (1kt/yr=1000 ton/year) and 13 kt/year, which are lower than the values 789 kt/yr and 635 kt/yr
247 respectively in Li et al.'s paper. The emissions of CO_2, CH_4 and N_2O increased significantly
248 from 2000 to 2014 in Jinan, mainly because of vehicle emissions (Sun et al., 2016). We use
249 the Sun et al.'s estimate of CO_2 and the ratio to estimate CO, about 1585 Gg/yr which is
250 similar with the value 1723 Gg/yr in 2014. Anthropogenic emissions dominate during winter
251 and spring. The temperature is very low in the winter and early spring, and the population
252 density is high, so the total energy consumption, especially coal, is very large during winter
253 and early spring (Zhao and Cui, 2014).
254
255 *3.3.2. Yellow Sea*
256 For the lower variability data the correlations are weak between every two gases. The
257 highest R^2 is 0.68 between ΔCO and ΔCH_4 but compared to other source regions it is still
258 weak. The average mole fractions enhancements of the four gases CO_2, CO, CH_4, N_2O in the
259 low-variability case were respectively 6.7 ppm, 110.4 ppb, 58.4 ppb, 0.28 ppb higher than the
260 base values. The number of data points in this case is high. The air masses tended to stay over

261 the Yellow Sea, so that there were much fewer high variability cases. Mixing of air masses
262 from different source regions, before our 72-hour back trajectories, may have weakened the
263 correlations. As expected, the relationships between the average enhancements for CO_2, CO,
264 and CH_4 corresponded to the values above, 6.7 ppm, 110.4 ppb, 58.4 ppb respectively, but not
265 for N_2O. Were the ratios of the average enhancements caused by regional emissions in China,
266 Korea, or do they came from larger areas as represented in MBL values? $\overline{\Delta CO}/\overline{\Delta CO_2}$=16.5
267 ppb/ppm, $\overline{\Delta CH_4}/\overline{\Delta CO_2}$= 8.7 ppb/ppm, and $\overline{\Delta CH_4}/\overline{\Delta CO}$= 0.5 ppb/ppb, whereas the MBL
268 latitudinal gradients between ~54 N and 30 N in 2017 during the same time were 3.7 ppb/ppm,
269 11.8 ppb/ppm, and 3.2 ppb/ppb respectively. Therefore the average enhancements are of
270 regional origin.
271
272 *3.3.3. Korea/Yellow*
273 In the lower variability case we have significant correlations between the hourly data for
274 ΔCO_2, ΔCO, and ΔCH_4, but not for ΔN_2O. The average mole fraction enhancements of the
275 four gases CO_2, CO, CH_4, N_2O are respectively 5.7 ppm, 105.4 ppb, 53.7 ppb, 0.28 ppb
276 higher than the base values, similar to the Yellow Sea case. There was relatively less CO than
277 in the Beijing case. Any influence from Korea appeared to be minor.
278
279 *3.3.4. Qingdao/Yantai/northeast*
280 The pair-wise correlations for the lower variability data look very similar to Beijing except
281 for ΔN_2O. All the R^2 values were above 0.8. The average mole fractions of the four gases CO_2,
282 CO, CH_4, N_2O are respectively 7.8 ppm, 127.5 ppb, 57.9 ppb, 0.61 ppb higher than the base

values. The air mass was mainly from northeast of China and then through Qingdao and Yantai. The back-trajectories fall in two groups. One group, the majority, stays mostly above 2 km and a small group stays below 500 m. In this case we may have had fairly clean air that picked up pollution at the end. The atmospheric CO_2 and CH_4 content observed at Longfengshan regional station (Fig.9) located in the northeast of China is influenced all year by anthropogenic emissions, and the mole fractions of CO_2 and CH_4 are higher in winter and spring. (Fang et al., 2017). The higher variability data show the same pair-wise correlations as the lower variability data for ΔCO_2, ΔCO, and ΔCH_4. The average enhancement of N_2O appears to be the highest, 4.4 ppb. The emissions of anthropogenic sources, including municipal solid waste, increased much in the northern provinces. Moreover, the landfill sites have contributed more significantly to the N_2O emissions in recent years in China (Du et al., 2017; Wang et al., 2017; Long et al., 2018).

3.3.5. Shanghai/Nanjing/Qingdao/northeast

The correlation relationships were relatively strong, all of them have R^2 above 0.8. Again back-trajectories stay mostly above 2 km, but near the end they went through several big cities of China. The air mass mainly went through the Yangtze River Delta (YRD) economic development zone where the economy is developed and the population is dense. Moreover, industrial emissions are mainly in Jilin and Liaoning provinces located in the northeast of China. Therefore the anthropogenic source contributed most in this case.(Pu et al., 2012; Cai et al., 2018). Moreover, Lixin Liu et al. found that the CO value at Shangdianzi (SDZ) station which is located near Beijing was considerably higher than CO at Linan (LAN) station which

is located in the center of the YRD region in spring (Liu et al., 2018), which is consistent with the observation in this study. The average mole fraction enhancements of the four gases CO_2, CO, CH_4, N_2O in the lower variability case are respectively 8.6 ppm, 113.6 ppb, 51.2 ppb, 0.77 ppb higher than the base values. For the higher variability data CH_4 is especially higher than the base value in this case, about 111.3 ppb. N_2O is also high, about 2.5 ppb higher than the base line. The correlation relationships are also relatively significant in the high variability case.

3.3.6. East China Sea

There are only lower variability data in this case. The R^2 values of the correlations between the hourly data of ΔCO_2, ΔCH_4 and ΔCO were not as high, like in the Yellow Sea case. The average mole fraction enhancements of the four gases CO_2, CO, CH_4, N_2O are respectively 4.9 ppm, 63.7 ppb, 42.8 ppb, 0.41 ppb higher than their corresponding base values. The ratios between these average enhancements are similar to the Yellow Sea case, and are thus a regional signature, not strongly polluted by any single source region.

3.3.7. Taiwan

For the lower variability data some of the correlation relationships are good, the R^2 are above 0.8, but not for $\Delta CH_4/\Delta CO_2$, $\Delta CH_4/\Delta CO$ and $\Delta N_2O/\Delta CH_4$, with R^2 values of about 0.36, 0.62 and 0.44 respectively. The average mole fraction enhancements of the four gases CO_2, CO, CH_4, N_2O are respectively 8.6 ppm, 85.5 ppb, 44.6 ppb, 0.95 ppb higher than the base values. The air came from Taiwan. The emissions of N_2O and CO_2 appear to be relatively

higher than the other two gas species. For the higher variability data the relationships of $\Delta N_2O/\Delta CO$ and $\Delta CO/\Delta CH_4$ are well-defined. Compared to other source regions, the pollution in Taiwan appears to be less than in several big cities in China, such as Beijing, Shanghai. The research of Chang and Lee (Chang and Lee, 2007) has shown that the air quality in Taipei City improved since 1994 according to the observation data from the monitoring stations established by the Taiwan Environmental Protection Administration.

3.3.8. Taiwan/Fuzhou/Wenzhou

There are much fewer lower variability data than higher variability data. The correlations of the data in this case are weak whether they are low or high variability data. The pollution came from several big cities along the coast. The contaminated air mass was not mixed evenly when it reached the measured point. The enhancement of CO_2 in this case is just below that from the source region of Beijing/Jinan.

3.3.9. Shanghai/Nanjing

There are only lower variability data in pair-wise comparisons of ΔCO_2, ΔCH_4, ΔCO and there are not enough data for ΔN_2O. The average mole fraction enhancements of the gases CO_2, CO, CH_4 are respectively 10.2 ppm, 105.4 ppb, 55.0 ppb higher than the base values. The correlations of $\Delta CO_2/\Delta CO$, $\Delta CO/\Delta CH_4$ are much better. The higher variability data only appear in the $\Delta N_2O/\Delta CO$ case, but there are only 6 data points. The correlation of $\Delta N_2O/\Delta CO$ is weak. There are high spikes of CO without high N_2O. In this case, the pollution was more concentrated.

3.3.10. North (Russia)

The correlations are not strong for the lower variability case. The air mass came from the North (Russia) and it also came from altitudes about 2 km. Near the end situation the altitude became low, and the air mass may have been influenced by some cities in China. The average mole fraction enhancements of the four gases CO_2, CO, CH_4, N_2O were respectively 8.6 ppm, 45.0 ppb, 52.0 ppb, 0.035 ppb higher than the base values. The ratios of the averages are on average closer to north-south gradients observed in the MBL, compared to the Yellow Sea and East China Sea. Compared with other source regions, the mole fractions of CO and N_2O in this case were the lowest.

4. Conclusions

Using the NOAA HYSPLIT model, the data were assigned to ten different source regions, which were mainly in North China and coastal cities of East China. We used two different methods to calculate the enhancement ratios of every pair of the gases and found that the enhancement ratio of $\Delta CH_4/\Delta CO$ is lower, and the enhancement ratio of $\Delta CO/\Delta CO_2$ is much higher in big cities like Beijing and Shanghai mainly because of the high CO emissions in these source regions in winter and early spring.

Compared with the MBL values of CO_2, CO, CH_4 and N_2O during the same time, the ratios of the average enhancements when the air had stayed over the Yellow Sea and the East China Sea for several days were caused by the emissions from the general region of Eastern China in

the spring. In this case the correlations of pairs of gases in every individual sample are weaker than for the urban source regions. For the source region called North (Russia) the enhancements ratios of the averages were on average closer to the MBL.

The methods used to calculate the enhancement ratios and the uncertainties of the ratios of the enhancements of every pair of gases in this study can be used to compare with emissions inventories as a completely independent check. Moreover, the observation data and the results can be used for multi-species inverse estimates of the sources and sinks of greenhouse gases (Pison et al., 2009; Wada et al., 2011). However, we want to emphasize that our observations of enhancement ratios do not depend on inverse modeling. Carefully calibrated data stand on their own, and will be "forever" if data management (archival) is handled correctly. We recommend that our approach be carried out in other seasons, to provide more comprehensive comparisons with emissions inventories.

Acknowledgments

This work was financially supported by the National Key Research and Development Program of China (Grant No.2016YFA0601304), the International S&T Cooperation Program of China (ISTCP: 2015DFG21960), the National Nature Science Foundation of China (Grant No. 41505123), and the CAMS Fundamental Research Funds (2015Y002).

We wish to thank the crew of the Dongfanghong II for their support. We feel grateful to the staffs at Beijing Huaxin Space＆Sky Technology Co., Ltd. (SST) for their technical support about the Picarro analyzers on the ship. We are thankful to the Carbon Cycle Greenhouse

Gases Group at Earth System Research Laboratory, National Oceanic and Atmospheric Administration (NOAA/ESRL) for guidance.

References

Boden, T., Andres, B., 2017. National CO_2 emissions from fossil-fuel burning, cement manufacture, and gas flaring:1751-2014. http://cdiac.ess-dive.lbl.gov/ftp/ndp030/nation.1751_2014.ems.

Butz, A., Guerlet, S., Hasekamp, O., Schepers, D., Galli, A., Aben, I., Frankenberg, C., Hartmann, J.M., Tran, H., Kuze, A., Keppel-Aleks, G., Toon, G., Wunch, D., Wennberg, P., Deutscher, N., Griffith, D., Macatangay, R., Messerschmidt, J., Notholt, J., Warneke, T., 2011. Toward accurate CO_2 and CH_4 observations from GOSAT. Geophys. Res. Lett. 38 (14), L14812.

Cai, B.F., Liang, S., Zhou, J., Wang, J.N., Cao, L.B., Qu, S., Xu, M., Y., Z.F., 2018. China high resolution emission database (CHRED) with point emission sources, gridded emission data, and supplementary socioeconomic data. Resour. Conserv. Recycl. 129, 232-239.

Chang, S.-C., Lee, C.-T., 2007. Evaluation of the trend of air quality in Taipei, Taiwan from 1994 to 2003. Environ. Monit. Assess. 127 (1-3), 87-96.

Chen, H., Winderlich, J., Gerbig, C., Hoefer, A., Rella, C.W., Crosson, E.R., Van Pelt, A.D., Steinbach, J., Kolle, O., Beck, V., Daube, B.C., Gottlieb, E.W., Chow, V.Y., Santoni, G.W., Wofsy, S.C., 2010. High-accuracy continuous airborne measurements of greenhouse gases (CO_2 and CH_4) using the cavity ring-down spectroscopy (CRDS) technique. Atmos. Meas. Tech. 3 (2), 375-386.

Cheng, S., An, X., Zhou, L., Tans, P.P., Jacobson, A., 2017. Atmospheric CO_2 at Waliguan station in China:

Transport climatology, temporal patterns and source-sink region representativeness. Atmos. Environ. 159, 107-116.

Crosson, E.R., 2008. A cavity ring-down analyzer for measuring atmospheric levels of methane, carbon dioxide, and water vapor. Appl. Phys. B 93 (3), 403-408.Daube, B.C., Boering, K.A., Andrews, A.E., Wofsy, S.C., 2002. A high-precision fast-response airborne CO_2 analyzer for in situ sampling from the surface to the middle stratosphere. J. Atmos. Oceanic Technol. 19 (10), 1532-1543.

Daube, B.C., Boering, K.A., Andrews, A.E., Wofsy, S.C., 2002. A high-precision fast-response airborne CO_2 analyzer for in situ sampling from the surface to the middle stratosphere. J. Atmos. and Oceanic Technol. 19 (10), 1532-1543.

Deng, F., Jones, D.B.A., Henze, D.K., Bousserez, N., Bowman, K.W., Fisher, J.B., Nassar, R., O'Dell, C., Wunch, D., Wennberg, P.O., Kort, E.A., Wofsy, S.C., Blumenstock, T., Deutscher, N.M., Griffith, D.W.T., Hase, F., Heikkinen, P., Sherlock, V., Strong, K., Sussmann, R., Warneke, T., 2014. Inferring regional sources and sinks of atmospheric CO_2 from GOSAT XCO_2 data. Atmos. Chem. and Phys. 14 (7), 3703-3727.

Ding, L.Y., Lu, Q.K., Xie, L.N., Liu, J., Cao, W., Shi, Z.X., Li, B.M., Wang, C.Y., Zhang, G.Q., Ren, S.X., 2016. Greenhouse gas emissions from dairy open lot and manure stockpile in northern China: A case study. J. Air Waste Manage. Assoc. 66 (3), 267-279.

Du, M.X., Peng, C.H., Wang, X.G., Chen, H., Wang, M., Zhu, Q., 2017. Quantification of methane emissions from municipal solid waste landfills in China during the past decade. Renew. Sustain. Energy Rev. 78, 272-279.

Erler, D.V., Duncan, T.M., Murray, R., Maher, D.T., Santos, I.R., Gatland, J.R., Mangion, P., Eyre, B.D., 2015. Applying cavity ring-down spectroscopy for the measurement of dissolved nitrous oxide concentrations and bulk nitrogen isotopic composition in aquatic systems: Correcting for interferences and field application. Limnol. Oceanogr.: Methods 13 (8), 391-401.

Fang, S.X., Zhou, L.X., Tans, P.P., Ciais, P., Steinbacher, M., Xu, L., Luan, T., 2014. In situ measurement of atmospheric CO_2 at the four WMO/GAW stations in China. Atmos. Chem. Phys. 14 (5), 2541-2554.

Fang, S.X., Tans, P.P., Yao, B., Luan, T., Wu, Y.L., Yu, D.J., 2017. Study of atmospheric CO_2 and CH_4 at Longfengshan WMO/GAW regional station: The variations, trends, influence of local sources/sinks, and transport. Sci. China Earth Sci. 60 (10), 1886-1895.

Feely, R.A., Takahashi, T., Wanninkhof, R., McPhaden, M.J., Cosca, C.E., Sutherland, S.C., Carr, M.-E., 2006. Decadal variability of the air-sea CO_2 fluxes in the equatorial Pacific Ocean. J. Geophys. Res. 111, C08S90.

Gomez-Pelaez, A.J., Ramos, R., Gomez-Trueba, V., Novelli, P.C., Campo-Hernandez, R., 2013. A statistical approach to quantify uncertainty in carbon monoxide measurements at the Izana global GAW station: 2008-2011. Atmos. Meas. Tech. 6 (3), 787-799.

GUM 1995, Guide to the expression of uncertainty in measurement, BIPM JCGM 100:2008

Guo, M., Li, J., Xu, J., Wang, X., He, H., Wu, L., 2017. CO_2 emissions from the 2010 Russian wildfires using GOSAT data. Environ. Pollut. 226, 60-68.

Han, J., Shin, B., Lee, M., Hwang, G., Kim, J., Shim, J., Lee, G., Shim, C., 2015. Variations of surface ozone at Ieodo Ocean Research Station in the East China Sea and the influence of Asian outflows. Atmos. Chem. Phys. 15 (21), 12611-12621.

Junker, C., Wang, J.-L., Lee, C.-T., 2009. Evaluation of the effect of long-range transport of air pollutants on coastal atmospheric monitoring sites in and around Taiwan. Atmos. Environ. 43 (21), 3374-3384.

Li, C.-X., Yang, G.-P., Wang, B.-D., Xu, Z.-J., 2016. Vernal distribution and turnover of dimethylsulfide (DMS) in the surface water of the Yellow Sea. J. of Geophys. Res. Oceans. 121 (10), 7495-7516.

Li, Y., Du, W., Huisingh, D., 2017. Challenges in developing an inventory of greenhouse gas emissions of Chinese cities: A case study of Beijing. J. Clean. Prod. 161, 1051-1063.

Liang, Q., Jaegle, L., Jaffe, D.A., Weiss-Penzias, P., Heckman, A., Snow, J.A., 2004. Long-range transport of Asian pollution to the northeast Pacific: Seasonal variations and transport pathways of carbon monoxide. J. Geophys. Res. 109, D23S07.

Liu, L., Zhou, L., Zhang, X., Wen, M., Zhang, F., Yao, B., Fang, S., 2009. The characteristics of atmospheric CO_2 concentration variation of four national background stations in China. Sci. China Ser. D-Earth Sci. 52 (11), 1857-1863.

Liu, L., Tans, P.P., Xia, L., Zhou, L., Zhang, F., 2018. Analysis of patterns in the concentrations of atmospheric greenhouse gases measured in two typical urban clusters in China. Atmos. Environ. 173, 343-354.

Long, X.E., Huang, Y., Chi, H.F., Li, Y.Y., Ahmad, N., Yao, H.Y., 2018. Nitrous oxide flux, ammonia oxidizer and denitrifier abundance and activity across three different landfill cover soils in Ningbo, China. J. Clean. Prod. 170, 288-297.

Machida, T., Matsueda, H., Sawa, Y., Nakagawa, Y., Hirotani, K., Kondo, N., Goto, K., Nakazawa, T., Ishikawa, K., Ogawa, T., 2008. Worldwide Measurements of Atmospheric CO_2 and Other Trace Gas Species Using Commercial Airlines. J. Atmos. and Oceanic Technol. 25 (10), 1744-1754.

Masarie, K.A. and P.P. Tans, Extension and integration of atmospheric carbon dioxide data into a globally consistent measurement record, J. Geophys. Res. 100, 11593-11610, 1995. Updated at www.esrl.noaa.gov/gmd/ccgg/mbl/

Moustafa, K., 2017. A clean environmental week: Let the nature breathe. Sci. Total Environ. 598, 639-646.

Peylin, P., Law, R.M., Gurney, K.R., Chevallier, F., Jacobson, A.R., Maki, T., Niwa, Y., Patra, P.K., Peters, W., Rayner, P.J., Roedenbeck, C., van der Laan-Luijkx, I.T., Zhang, X., 2013. Global atmospheric carbon budget: results from an ensemble of atmospheric CO_2 inversions. Biogeosciences. 10 (10), 6699-6720.

Pison, I., Bousquet, P., Chevallier, F., Szopa, S., Hauglustaine, D., 2009. Multi-species inversion of CH_4, CO and

481 H_2 emissions from surface measurements. Atmos. Chem. Phys. 9 (14), 5281-5297.

482 Pu, J., Xu, H., Gu, J., Zhou, L., Fang, S., 2012. Study on the concentration variation of CO_2 in the background area

483 of Yangtze River Delta. China Environ. Sci. 32(6), 973-979. (in Chinese with English abstract).

484 Sakata, M., Ishikawa, T., Mitsunobu, S., 2013. Effectiveness of sulfur and boron isotopes in aerosols as tracers of

485 emissions from coal burning in Asian continent. Atmos. Environ. 67, 296-303.

486 Sawa, Y., Machida, T., Matsueda, H., 2012. Aircraft observation of the seasonal variation in the transport of CO_2 in

487 the upper atmosphere. J. Geophys. Res. 117, D05305.

488 Schuster, U., Watson, A.J., Bates, N.R., Corbiere, A., Gonzalez-Davila, M., Metzl, N., Pierrot, D., Santana-Casiano,

489 M., 2009. Trends in North Atlantic sea-surface fCO_2 from 1990 to 2006. Deep-Sea Research II. 56 (8-10),

490 620-629.

491 Sun, S.D., Jiang, W., Gao, W.D., 2016. Vehicle emission trends and spatial distribution in Shandong province,

492 China, from 2000 to 2014. Atmos. Environ. 147, 190-199.

493 Suntharalingam, P., Jacob, D.J., Palmer, P.I., Logan, J.A., Yantosca, R.M., Xiao, Y.P., Evans, M.J., Streets, D.G.,

494 Vay, S.L., Sachse, G.W., 2004. Improved quantification of Chinese carbon fluxes using CO_2/CO correlations

495 in Asian outflow. J. Geophys. Res. 109, D18S18.

496 Tans, P., and C. Zellweger., 2014. Editors, 17th WMO/GAW Meeting on Carbon Dioxide, Other Greenhouse Gases

497 and Related Tracers Measurement Techniques. WMO/GAW Report, No. 213: 1-43.

498 Wada, A., Matsueda, H., Sawa, Y., Tsuboi, K., Okubo, S., 2011. Seasonal variation of enhancement ratios of trace

499 gases observed over 10 years in the western North Pacific. Atmos. Environ. 45 (12), 2129-2137.

500 Wada, A., Sawa, Y., Matsueda, H., Taguchi, S., Murayama, S., Okubo, S., Tsutsumi, Y., 2007. Influence of

501 continental air mass transport on atmospheric CO_2 in the western North Pacific. J. Geophys. Res. 112,

502 D07311.

503 Wang, X.J., Jia, M.S., Zhang, C.L., Chen, S.H., Cai, Z.C., 2017. Leachate treatment in landfills is a significant N_2O
504 source. Sci. Total Environ. 596-597, 18-25.
505 Wunch, D., Wennberg, P.O., Osterman, G., Fisher, B., Naylor, B., Roehl, C.M., O'Dell, C., Mandrake, L., Viatte, C.,
506 Kiel, M., Griffith, D.W.T., Deutscher, N.M., Velazco, V.A., Notholt, J., Warneke, T., Petri, C., De Maziere, M.,
507 Sha, M.K., Sussmann, R., Rettinger, M., Pollard, D., Robinson, J., Morino, I., Uchino, O., Hase, F.,
508 Blumenstock, T., Feist, D.G., Arnold, S.G., Strong, K., Mendonca, J., Kivi, R., Heikkinen, P., Iraci, L.,
509 Podolske, J., Hillyard, P., Kawakami, S., Dubey, M.K., Parker, H.A., Sepulveda, E., Garcia, O.E., Te, Y.,
510 Jeseck, P., Gunson, M.R., Crisp, D., Eldering, A., 2017. Comparisons of the Orbiting Carbon Observatory-2
511 (OCO-2) X_{CO2} measurements with TCCON. Atmos. Meas. Tech. 10 (6), 2209-2238.
512 Zellweger, C., Emmenegger, L., Firdaus, M., Hatakka, J., Heimann, M., Kozlova, E., Spain, T.G., Steinbacher, M.,
513 van der Schoot, M.V., Buchmann, B., 2016. Assessment of recent advances in measurement techniques for
514 atmospheric carbon dioxide and methane observations. Atmos. Meas. Tech. 9 (9), 4737-4757.
515 Zhang, N., Bai, Z., Luo, J., Ledgard, S., Wu, Z., Ma, L., 2017. Nutrient losses and greenhouse gas emissions from
516 dairy production in China: Lessons learned from historical changes and regional differences. Sci. Total
517 Environ. 598, 1095-1105.
518 Zhao, J., Cui, W.H., 2014. Spatial and Temporal Distribution Characteristics of CO_2 Column Concentration in
519 China from 2009 to 2010. J. Geo-information Sci. 16(2), 207-213. (in Chinese with English abstract).
520

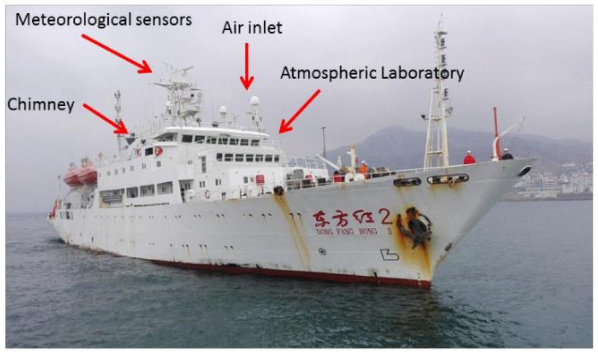

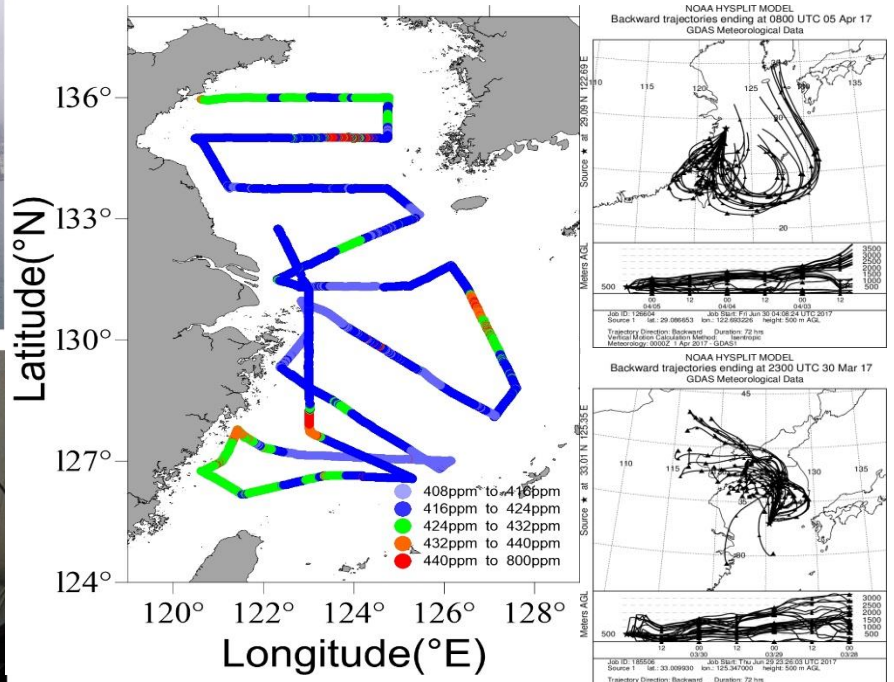

Mole fraction distribution of CO_2

A ship-board continuously observation system was applied to observe the atmospheric distributions of CO_2, CO, CH_4 and N_2O over the Yellow Sea and the East China Sea and we obtained the high-precision data to analyze the source regions through the NOAA HYSPLIT Model and study the emission characteristics of these areas.